An Energetic Approach to Task-Invariant Ankle Exoskeleton Control

Katharine Walters[1], Gray C. Thomas[1], Jianping Lin[2], and Robert D. Gregg[1]

***Abstract*— Robotic ankle exoskeletons have been shown to reduce human effort during walking. However, existing ankle exoskeleton control approaches are limited in their ability to apply biomimetic torque across diverse tasks outside of the controlled lab environment. Energy shaping control can provide task-invariant assistance without estimating the user's state, classifying task, or reproducing pre-defined torque trajectories. In previous work, we showed that an optimally task-invariant energy shaping controller implemented on a knee-ankle exoskeleton reduced the effort of certain muscles for a range of tasks. In this paper, we extend this approach to the sensor suite available at the ankle and present its implementation on a commercially-available, bilateral ankle exoskeleton. An experiment with three healthy subjects walking on a circuit and on a treadmill showed that the controller can approximate biomimetic profiles for varying terrains and task transitions without classifying tasks or switching control modes.**

I. Introduction

Robotic ankle exoskeletons have the potential to assist people in their daily lives. The ankle plantar-flexor muscles contribute 77% of positive work during the push-off phase of gait [1] and 27% of total muscle energy expenditure over the gait cycle [2]. As the ankle makes significant contributions to ambulation, actively augmenting human plantar-flexor muscles can reduce human effort [3]. However, human ambulation is highly complex and providing biomimetic ankle assistance across the various activities of daily living (ADLs) remains a challenge.

Directly measuring human plantar-flexor muscle activation to control exoskeleton assistance offers an intuitive manner to control different activities. There has been some success in mapping muscle activation, measured with electromyography (EMG) sensors, to exoskeleton assistance through proportional gains [4], [5] or using muscle activation as human-in-the-loop control inputs to guide the development of assistive torque profiles [6] for level treadmill walking. However, EMG sensors are inherently noisy, sensitive to placement, motion and alterations to the user's muscle recruitment strategy [7], and the heavy filtering required [4]–[6] is not practical for providing assistance across highly variable ADLs.

This work was supported by the National Science Foundation Graduate Research Fellowship under Award Number 1841052 and by the National Institute of Biomedical Imaging and Bioengineering of the NIH under Award Number R01EB031166. The content is solely the responsibility of the authors and does not necessarily represent the official views of the NSF or NIH. (Corresponding author: Robert D. Gregg.)

[1]Katharine Walters, Gray Thomas, and Robert D. Gregg are with the Department of Robotics, University of Michigan, Ann Arbor, MI 48109, USA. {kwalte, gcthomas, rdgregg}@umich.edu

[2]Jianping Lin is with the State Key Laboratory of Mechanical System and Vibration, School of Mechanical Engineering, Shanghai Jiao Tong University, Shanghai 200240, China. {jplin}@umich.edu

Many ankle exoskeleton controllers in the literature have successfully reduced metabolic cost or muscular effort during gait by applying pre-defined torque trajectories as a function of time between heel-strikes [8]–[14]. These timing-based estimation (TBE) approaches have shown promising results in the lab by optimizing different parameters of biomimetic ankle torque profiles, including timing of actuation onset [8], [9], the collection of rise time, torque peak timing, torque peak magnitude, and fall time parameters [11], [12], total positive exoskeleton power [9], [10], total negative exoskeleton power [10], net work [13], or average torque [13]. However, TBE is sensitive to changes in speed and pre-defined torque trajectories are rarely appropriate for the highly variable terrains and tasks outside of the controlled lab environment. One recent approach has attempted to augment TBE with speed adaptation at each heel-strike to improve efficacy in uncontrolled environments [14], but sudden accelerations remain a fundamental problem to TBE.

To provide more accurate torque assistance under speed variations and overcome the drawbacks of TBE, phase-estimation approaches continuously track gait progression from heel-strike to heel-strike and map phase to the instantaneous desired torque. Machine learning phase estimators have outperformed TBE in predicting gait events (i.e., heel-strike and toe-off) and applying biomimetic ankle torque profiles for sinusoidally varying level walking speeds [15], while being robust to transitions between walking and standing [16]. Phase has also been used to differentiate between walking, running, and jumping tasks and map to the appropriate torque profiles [17]. Further, an Extended Kalman Filter estimating phase states alongside task states successfully adapted biomimetic torque profiles over continuously varying speeds and highly uneven terrains without explicitly classifying the task [18]. However, controllers that require state estimation or classification have the potential to apply unexpected torques if the state or task are misidentified, which can impact the user's perception of device reliability.

Task-invariant controllers provide assistance without estimating the user's state, classifying task, or relying on pre-defined torque trajectories. For example, a recent task-invariant ankle exoskeleton controller provides assistance proportional to the force at the ball of the foot [19]. However, this method of direct force amplification has an intrinsic trade-off between sensitivity required to quickly respond to the user's voluntary movement and robustness to variation in model parameters and control inputs [20]. Energy shaping provides an alternative task-invariant control framework that alters the energetic properties of the target system using kinematic control inputs. Previously implemented on

an ankle-foot orthosis, potential energy shaping provided task-invariant virtual body-weight support for rehabilitation [21]. To increase the amount of assistance, another energy-shaping control law was parameterized with basis functions depending on actuated joint angles and optimized based on able-bodied kinematic/kinetic data over a range of walking inclines [22]. However, by only depending on the actuated joint coordinates, the controller was limited to virtual spring-like behaviors that cannot provide appropriate assistance for more diverse activities like stair climbing.

To increase flexibility to reproduce biomimetic torques across ADLs, the optimal energy shaping framework was extended to incorporate vertical ground reaction force and global orientation [23]. This optimization-based control law implemented on a knee-ankle exoskeleton reduced the effort of certain muscles for a range of tasks including walking, ramps, and stairs. This previous work used the global thigh angle as an input to the control law to help differentiate torque predictions between activities, but this sensor input is not available to a self-contained ankle exoskeleton. Moreover, this study neglected to assess controller performance over transitions between activities, which were not explicitly designed into the controller but occur frequently in daily life.

The contributions of this paper include extending the optimal task-invariant energy shaping framework to a single-joint ankle exoskeleton without relying on sensor information proximal to the shank or information from the contralateral leg. The controller is implemented and validated on a commercially available ankle exoskeleton, bringing this technology one step closer to market. An experiment with three able-bodied subjects walking on a circuit and a treadmill shows that the controller approximates biomimetic torque profiles for varying terrains without classifying tasks or switching control modes. This paper further validates the ability of this control approach to approximate biomimetic torques during task transitions that are outside of the training set.

II. Review of Energy-Shaping Framework

This section models the human-exoskeleton system with signals local to the ankle and reviews the energy-shaping framework presented in detail in [23].

A. System Modelling

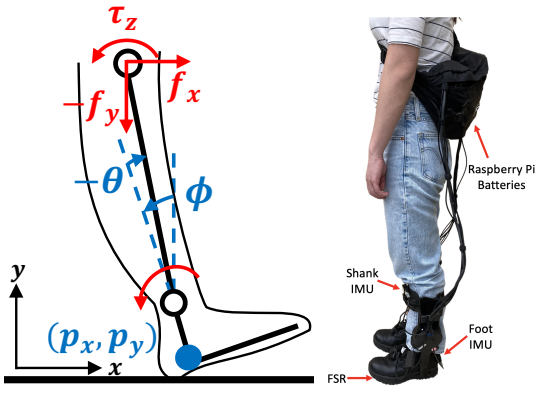

Fig. 1. System model (modified from [23]) and commercial ankle exoskeleton hardware setup.

The human-exoskeleton system comprises inertia of the human rigidly coupled to the torque production capabilities of the exoskeleton. The system is modeled with two links representing the shank and foot and one revolute joint (Fig. 1). The global heel angle ϕ is defined relative to gravity and the foot, and θ is the relative ankle angle (independent of ϕ). The Cartesian coordinates of the heel are given by (p_x, p_y). We focus the model on the stance leg, for which the ankle primarily applies plantarflexion torque. The four degrees-of-freedom (DOF) model has the generalized coordinates $q = [p_x, p_y, \phi, \theta]^T \in \mathbb{R}^4$. The body interaction forces influence the dynamics of the system through $F = [f_x, f_y, \tau_z]^T$. The conjugate momenta is given by $p = M(q)\dot{q} \in \mathbb{R}^4$, where $M(q) \in \mathbb{R}^{4\times4}$ is the positive definite inertia matrix and $\dot{q} \in \mathbb{R}^4$ is the velocity vector.

We define the dynamics as a Hamiltonian system, as in [23], where evolution of q and p is linear in the gradient of total energy, H, and two external inputs, τ and λ, as

$$\begin{bmatrix}\dot{q}\\ \dot{p}\end{bmatrix} = \begin{bmatrix}0_{4\times4} & I_{4\times4}\\ -I_{4\times4} & 0_{4\times4}\end{bmatrix}\nabla H + \begin{bmatrix}0\\ \tau + A^T\lambda\end{bmatrix}, \tag{1}$$

where total energy is given by the Hamiltonian function $H(p,q) = \frac{1}{2}p^T M^{-1}(q)p + V(q)$, where the quadratic term is the kinetic energy and $V(q)$ is potential energy. The joint torques $\tau = \tau_{\text{exo}} + \tau_{\text{hum}} \in \mathbb{R}^4$ aggregate the exoskeleton and human inputs, respectively, where $\tau_{\text{exo}} = Bu$ and $\tau_{\text{hum}} = Bv + J(q)^T F$. The exoskeleton control torque $u \in \mathbb{R}$ and human ankle torque $v \in \mathbb{R}$ are mapped into the 4-dimensional coordinate space by matrix $B = [0_{1\times3}, 1]^T$, and F is mapped through the shank-tip Jacobian $J(q) \in \mathbb{R}^{3\times4}$. The ground reaction forces (GRFs), represented by the Lagrange multiplier $\lambda \in \mathbb{R}^c$, are mapped into the equation through the constraint matrix $A \in \mathbb{R}^{c\times4}$, where c is the number of contact constraints. As the generalized coordinates outnumber the actuated coordinates, the system is underactuated.

B. Control Law

We consider the desired closed-loop Hamiltonian $\widetilde{H}(p,q) = \frac{1}{2}p^T \widetilde{M}^{-1}(q)p + \widetilde{V}(q)$, where the desired potential energy $\widetilde{V} = V + \widehat{V}$ depends on the shaping term $\widehat{V}$. The corresponding gravitational vector is $\widetilde{N} = \nabla_q \widetilde{V} = N + \widehat{N} \in \mathbb{R}^4$. We set $\widetilde{M} = M$ to avoid requiring acceleration feedback or unrealistic knowledge of τ_{hum} to change the mass matrix in the control law. The desired dynamics are

$$\begin{bmatrix}\dot{q}\\ \dot{p}\end{bmatrix} = \begin{bmatrix}0_{4\times4} & I_{4\times4}\\ -I_{4\times4} & 0_{4\times4}\end{bmatrix}\nabla \widetilde{H} + \begin{bmatrix}0\\ Bv + J(q)^T F + A^T\widetilde{\lambda} + B_x u_x\end{bmatrix}, \tag{2}$$

where $\widetilde{\lambda}$ represents the closed-loop GRFs, and the external input $u_x \in \mathbb{R}$ allows unactuated global angle information to shape the dynamics of the actuated joint as explained in Sec. II-C. The matrix $B_x = [0,0,1,0]^T$ restricts u_x to only act on the global angle ϕ. With only one actuated degree of freedom, the skew-symmetric interconnection matrix has no free parameters. Thus, $\nabla\widetilde{H} = \nabla H + [\nabla_q \widehat{V}, 0]^T$, and only potential energy terms in ϕ and θ are added.

The Hamiltonian systems (1) and (2) match if

$$\begin{aligned} Bu &= -(\nabla_q \widetilde{H})^T + (\nabla_q H)^T + A^T(\widetilde{\lambda} - \lambda) + B_x u_x \\ &= -\widetilde{N} + N + A^T(\widetilde{\lambda} - \lambda) + B_x u_x. \end{aligned} \tag{3}$$

Following the steps in [23], the matching conditions are satisfied when the unactuated parts of $-\widetilde{N} + N + B_x u_x$ are set equal to zero. A feasible control law satisfying the matching conditions given in (3) is

$$\begin{aligned} u &= B^+\{-(\nabla_q \widetilde{H})^T + (\nabla_q H)^T + B_x u_x\} \\ &= B^+\{-\widetilde{N} + N + B_x u_x\} = B^+\{-\widehat{N} + B_x u_x\}, \end{aligned} \tag{4}$$

where $B^+ = (B^T B)^{-1} B^T$ is the left pseudo-inverse of B.

C. Passivity and Stability

Without including the external input $B_x u_x$ in the matching conditions, the modified gravitational vector $\widehat{N}$ can depend only on the actuated coordinate θ. This restricts the controller to non-linear virtual spring behaviors about the ankle. Thus, to increase control flexibility, we use the relaxation term $B_x u_x$ to allow the control law to make use of the unactuated global angle signal, ϕ. This results in a "power leak" in our target system that is small compared to the human contribution, and stability of the human-exoskeleton system is maintained through human impedance control [23].

III. Control Optimization

To design a task-invariant controller that satisfies matching conditions, we apply an optimization over a basis-function representation of the space of possible controllers, where each basis satisfies the relaxed matching conditions. Simulation results then verify that the resulting controllers approximate biological torque across all the considered ADLs.

A. Basis Functions

To reformulate the control law (4) as an optimization problem, we define $\widehat{N} = [0, 0, 0, -\alpha_1\zeta_1 - \ldots - \alpha_w\zeta_w]^T \in \mathbb{R}^4$ as a linear combination of basis functions $\zeta_i \in \mathbb{R}$ with constant coefficients α_i for $i = 1, \ldots, w$, where w is the total number of bases. The basis functions, defined by the set

$$\begin{aligned} \zeta = \{&1, \psi, \sin(\psi), \cos(\psi), \sin(2\psi), \cos(2\psi), \\ &\phi, \sin(\phi), \cos(\phi), \sin(2\phi), \cos(2\phi)\}, \end{aligned}$$

are intuitively chosen as trigonometric functions of ϕ and the global shank orientation $\psi = \phi - \theta$. The basis functions are integrable to ensure the closed-loop system has a well-defined potential energy. The controller output is also bounded through the nature of the basis functions, with the global orientations ϕ and ψ bounded $[-\pi, \pi]$ and the trigonometric functions bounded $[-1, 1]$. To taper the torque during the double-support phase, the vertical ground reaction force $vGRF \in \mathbb{R}$, normalized to 100% bodyweight, is incorporated into the control law as

$$u = \beta(vGRF) \cdot vGRF \cdot B^+ \widehat{N} = U(q, vGRF)\alpha, \tag{5}$$

where $B^+ = [0_{1\times 3}, 1]^T$, $\alpha \in \mathbb{R}^{w\times 1}$, and $\beta \in \mathbb{R}$ is a sigmoid function of $vGRF$ that zeros the control torque below 10% bodyweight during stance and swing transitions.

This small set of basis functions minimizes control law complexity while capturing fundamental relationships between kinematics and ankle torque (Fig. 2). With the exception of ϕ, $\sin(\phi)$ and $\sin(2\phi)$, which peak at toe-off, all basis functions have a peak at roughly 80% of the stance phase. This peak roughly coincides with the push-off torque impulse. The raw global angle ϕ provides an indicator of ground incline during mid-stance when the foot is flat. The bases ϕ and $\sin(2\phi)$ are zero in mid-stance for level walking and stair tasks. As a result, functions ϕ and $\sin(2\phi)$ can appropriately increase or decrease torque for ramps without impacting other tasks. The global shank angle provides critical information about phase for all tasks, as noted in [17], [25]. For example, the shape of $\sin(2\psi)$ indicates the presence of a torque peak during loading response at roughly 20% of stance for ramp decline and stair descent/ascent in contrast to level walking and ramp incline.

B. Optimization Formulation

We optimized the control parameters to minimize the error between control torques and normative human torques. The optimization problem is defined as

$$\begin{aligned} \underset{\alpha, s}{\text{minimize}} \quad & \sum_j \Big[C_j + s + \Lambda \|W_s \alpha\|_1 \Big], \\ \text{subject to} \quad & C_j = (U_j\alpha - Y_j)^T W_j (U_j\alpha - Y_j), \\ & s \geq -Y_j^T U_j \alpha, \quad s \geq 0, \end{aligned}$$

where j represents the task being optimized, $Y_j \in \mathbb{R}^{m\times 1}$ is the normative human torque with m data samples for each task, and the matrix $U_j = U(q_j, vGRF_j) \in \mathbb{R}^{m\times w}$ represents the basis evaluated at each time element along j with state vector $q_j = [\phi, \psi] \in \mathbb{R}^{m\times 2}$.

The first term of the optimization cost penalizes the squared error between the controller torque U_j and the normative human torque Y_j. The tasks j are weighted according to matrix W_j, where the level treadmill walking tasks are weighted higher than all other tasks to prioritize walking performance as the most frequent ADL. The second cost term minimizes controller torque of the opposite sign of normative torque Y_j to ensure that the control torque does not resist the user. If the normative torque is of an opposite sign of the predicted torque, then s takes on a positive value, which the optimization seeks to minimize. If there are no wrong torque signs, then s is constrained to be zero and it has no effect on the optimization. The final cost term L1-regularizes α with weight matrix W_s to minimize over-fitting. The optimization problem was solved using the `cvx` convex optimization package in MATLAB [26].

The optimization used the intra-subject average steady-state stride for each of 12 able-bodied subjects for level treadmill walking at 0.5m/s and 1.5m/s, ramp incline and decline at 5.2° and 11°, and stair ascent and descent for 4 and 7 inch step heights [24]. Average stand-to-sit data was obtained from a separate source [27] and repeated for each subject in the primary dataset so the optimization problem had the same number of each task. The second complete

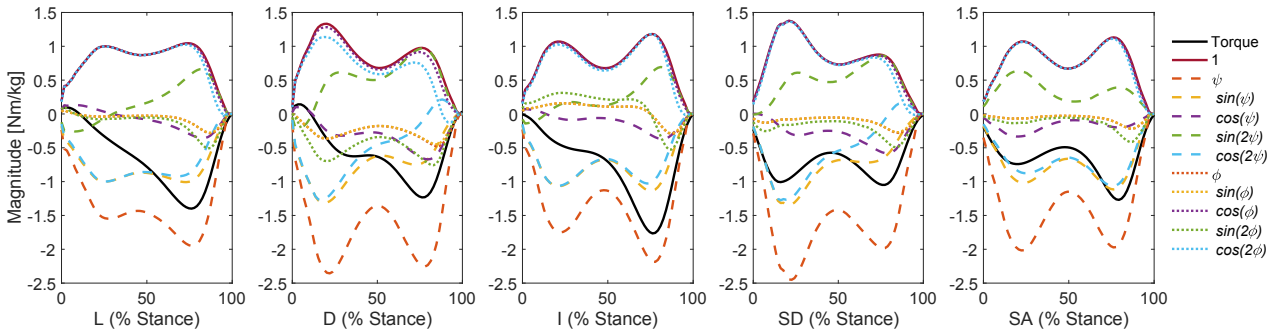

Fig. 2. **Basis functions ζ, scaled by vGRF**, plotted from average able-bodied input data for 1 m/s walking (L), 11° ramp decline (D) and incline (I), and 7 inch stairs descent (SD) and stairs ascent (SA), compared to the average joint torque from dataset [24]. Function ϕ closely tracks $\sin(\phi)$.

stride (occurring heel-strike to heel-strike) on the ramp and stair was treated as the steady-state stride, as it was not one of the first two transitioning strides and had kinetics available.

C. Simulation Validation

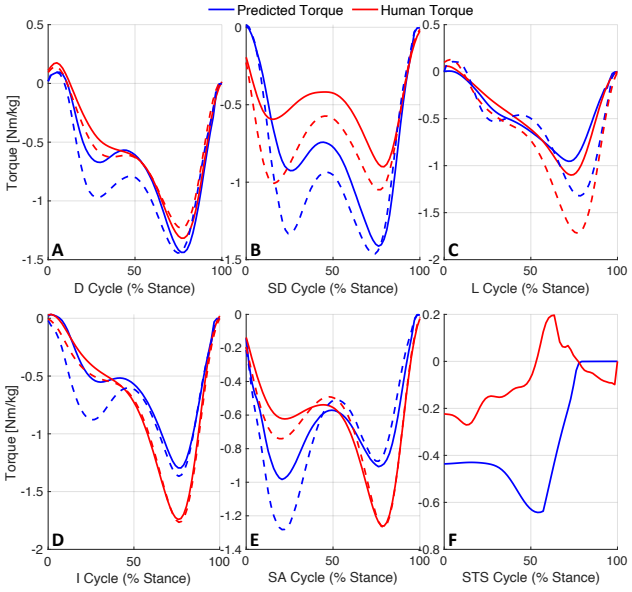

Fig. 3. **Simulated controller torque vs. normative human torque** in stance, across 5.2° (solid) and 11° (dashed) ramp decline (D), 5.2° (solid) and 11° (dashed) ramp incline (I), 4 inch (solid) and 7 inch (dashed) stairs descent (SD), 4 inch (solid) and 7 inch (dashed) stairs ascent (SA), 0.5 m/s (solid) and 1.5 m/s (dashed) level walking (L) and stand-to-sit (STS). Note that human ankle torque is small during STS, reducing the importance of that task's lower prediction quality.

The controller was simulated with the average kinematics of the 12 subjects used to optimize the torque parameters (Fig. 3). To evaluate the predicted torques in comparison to normative, we used the performance metrics Cosine Similarity (SIM) and Variance Accounted For (VAF) as in [23]:

$$\mathrm{SIM}(A,B) = \frac{100 \cdot A \cdot B}{\|A\|_2 \|B\|_2} \ ,$$

$$\mathrm{VAF}(A,B) = 100 \cdot \left[1 - \frac{\mathrm{var}(A-B)}{\mathrm{var}(A)}\right] \ ,$$

where A is normative torque and B is predicted torque. We calculated SIM and VAF across all subjects for each task using the optimized parameters (Fig. 4, "Nominal").

Leave-one-subject-out and leave-one-task-out validation was performed to test the sensitivity of controller performance to the subject and task data included in the optimization. In leave-one-subject-out validation, we calculated the SIM and VAF for a single subject's normative torque in comparison to predicted torque for all tasks using parameters optimized without that subject's data (see Fig. 4, "Subject"). In leave-one-task-out validation, we calculated the SIM and VAF for each subject's normative torque in comparison to predicted controller torque for a single task using parameters optimized without that task (see Fig. 4, "Task"). The stand-to-sit task was left out because only one average sample was available to use in the optimization.

The simulated controller has the best performance for walking tasks, with phase-aligned normative and predicted torque peaks (Fig. 3.C) resulting in high SIM and predicted torque peaks of roughly correct magnitude resulting in high VAF (Fig. 4.C1,C2). The predicted torque for ramp tasks also aligns very well with normative, though there is some discrepancy in magnitude, with slightly higher predicted peak magnitude in ramp decline and lower predicted peak magnitude for ramp incline (Fig. 3.A,D). The predicted torque for the steeper incline ramp tasks has a higher peak during the transition from loading response to mid-stance (i.e., roughly 25% stance) compared to normative, resulting in slightly lower SIM compared to the shallower incline (Fig. 4.A2,D2). Steeper inclines also have lower median VAF and larger variance across subjects compared to level walking, resulting from varying magnitudes of predicted loading response and push-off torque peaks across subjects.

In stair tasks, the simulated controller applied torque peaks at the end of loading-response and at push-off (Fig. 3.B,E). For some subjects, stair task loading response torque peak magnitudes are over-predicted while the push-off torque peak magnitudes are under-predicted, resulting in higher variance for the difference between normative and predicted compared to normative variance. The resulting negative VAF value for some stair tasks results in low median VAF (Fig. 4.B1,B2). Despite the low VAF, the high SIM indicates that the controller correctly predicts the phase alignment of assistive torque peaks across subjects. Predicted torque for stand-to-sit has opposite sign compared to normative. However, human ankle torque is small during stand-to-sit, so this torque mismatch (Fig. 3.F) is less consequential.

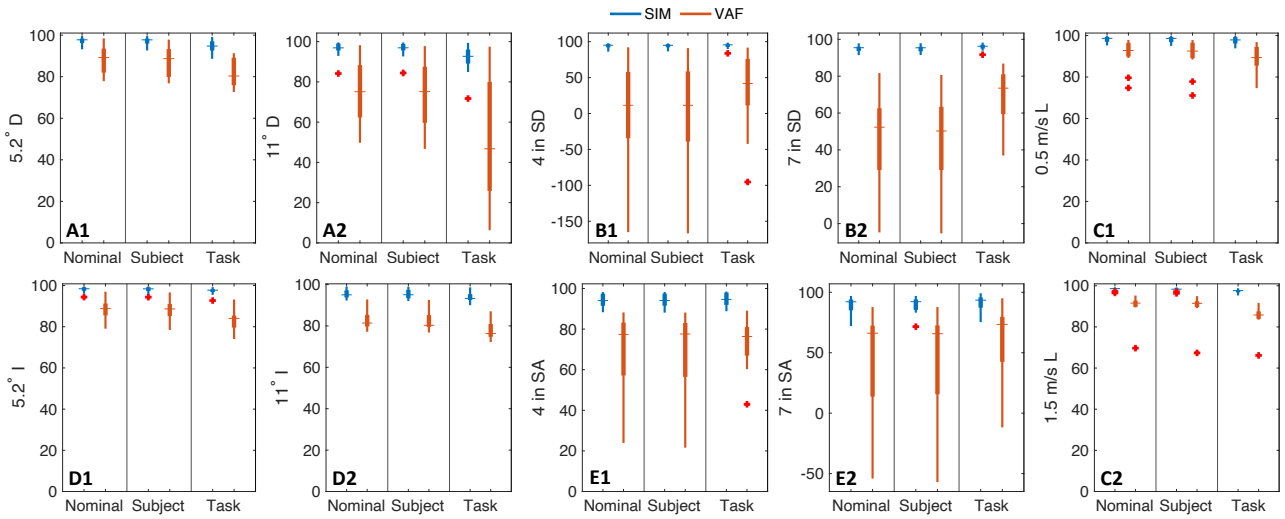

Fig. 4. **SIM and VAF results for the simulated controller** with all subjects across tasks (Nominal), leave-one-subject-out across tasks (Subject), and leave-one-task-out across subjects (Task) for ramp incline (I), ramp decline (D), stairs descent (SD), stairs ascent (SA) and level walking (L).

Leave-one-subject-out and leave-one-task-out resulted in high SIM across tasks (Fig. 4). With the exception of the slight decrease in SIM when leaving out the 5.2° ramp decline and 11° ramp incline and decline, the SIM values are roughly constant when leaving subjects and tasks out of the optimization compared to Nominal. The consistent SIM results show that the phase alignment of the assistance torque peaks is not sensitive to the data included in the optimization. The VAF results for leaving subjects out of the optimization are also very similar to Nominal, indicating that controller variance is not sensitive to subject-specific data. However, leaving ramp and walking tasks out of the optimization leads to lower VAF results while leaving stair tasks out results in better performance with higher median VAF or smaller VAF distributions. This decrease in VAF is likely because kinematics/kinetics vary across inclines, and the diverse inclines included in the optimization captured the variability between tasks necessary to accurately approximate torque for those tasks. The number of walking and ramp tasks included could also have weighted the optimization in favor of correctly approximating torque for those tasks, and when they are left out, the optimization is improperly weighted toward stair tasks. The kinematics/kinetics for stair tasks are highly variable across subjects, so the increase in VAF when leaving out stair tasks is likely because the optimization no longer attempts to optimize a limited number of torque parameters to predict torque for diverse subjects.

Though the global angles and *vGRF* included in the framework improve the flexibility to provide biomimetic torques across tasks, the lack of information proximal to the shank decreases the accuracy of the controller in approximating torque magnitudes for ascent versus descent tasks. However, the high SIM across subjects for all tasks indicates that users can expect assistance at the correct phase for all tasks.

IV. Human Subject Proof-of-Concept Validation

This section presents the task-invariant controller implementation on a commercially available ankle exoskeleton and experimental validation with N=3 human subjects.

A. Hardware Implementation

The controller was implemented on left and right units of the Dephy EB51 ExoBoot (Dephy MA, USA), Fig. 1. The ExoBoot exerts plantarflexion torque via a brushless motor that spools an inelastic belt rigidly attached to a lever arm connected to the ankle joint. The maximum ankle torque is 30Nm. The amount of belt spooled around the motor and the angle of the ankle joint and lever arm relative to the motor result in a variable transmission ratio. The gear ratio through the normal ankle range of motion is roughly 15:1. Two inertial measurement units (IMUs) attached to the shank cuff and heel of the boot provided the global shank angle and global foot angle (3DM-GX5-25, Lord MicroStrain). A commercial insole pressure sensor (FSR) measured vGRF (Actisense, IEE, Luxembourg). Each ExoBoot was controlled with a Raspberry Pi 4B with 8GB RAM. Each unilateral system was powered with one 24V, 2.0 Ah lithium-ion battery (Kobalt). Each unilateral system weighed 2 kg.

As the ExoBoot uses a plantarflexion-only belt drive, a state machine used the vGRF (normalized by user mass between 0 for swing and 1 for single-support stance) to switch control modes when transitioning between stance and swing. During swing, the motor was position-controlled to maintain belt slack, to allow the user to dorsiflex freely without feeling the motor's inertia. The same behavior was controlled in stance when the controller commanded a dorsiflexion torque. When the controller commanded a plantarflexion torque during stance, the motor was given a current command calculated as a function of the desired torque, the gear ratio as a function of the instantaneous ankle angle, and the motor current constant. The control torque calculated from (5) was multiplied by the user's mass and preferred percent level of torque assistance (%LOA). For user comfort and to account for FSR error, plantarflexion torque was softened by a sigmoid function of vGRF during transitions between stance and swing.

B. Experiment Method

To validate the performance of the controller in providing biomimetic torques across a range of ADLs, N=3 able-bodied participants (AB1: male, 75 kg, 1.88 m; AB2: female, 61 kg, 1.69 m; AB3 = male, 85 kg, 1.78 m) completed ambulation ADLs on a circuit and on a treadmill while wearing bilateral ankle exoskeletons. The study was approved by the University of Michigan IRB under protocol HUM00201957. The circuit consisted of a ramp inclined at 14.1°, a level platform, stairs with 7 inch step height, and space to walk on level ground to return to the starting position. Clockwise (CW) circuits consisted of standing, ramp incline, stairs decline, level walking, and returning to sitting. Counter-clockwise (CCW) circuits consisted of standing, level walking, stairs incline, ramp decline, and returning to sitting.

Participants were given time to acclimate to the exoskeleton assistance and find their preferred %LOA while practicing over the circuit. During acclimation, each participant traversed the circuit roughly five times in each direction and walked on a treadmill for roughly a minute at speeds of 1m/s, 1.25m/s, and 0.75m/s until appropriate comfort with the exoskeleton assistance was achieved. During the training sessions, participants were allowed to use handrails, but during the experiment the handrails were disallowed. During data collection, participants began each circuit seated and alternated traversing the circuit in CW or CCW directions at a self-selected speed for a total of ten times in each direction. Participants were then asked to walk on an instrumented treadmill (Bertec, Columbus, OH) for two minutes at each of three speeds: 1 m/s, 1.25 m/s, and 0.75 m/s.

Control performance was validated using the control torque (Nm) desired at the ankle and not the output ankle torque (Nm) calculated with motor current, as the intent was to validate the controller and not the hardware. The low mean (μ) and maximum (max) root-mean squared error for control torque compared to output torque for steady-state strides indicates that error in output torque did not have a significant impact the user's gait (AB1: μ = 0.76, max = 3.66 Nm; AB2: μ = 1.11, max = 3.28 Nm; AB3: μ = 0.97, max = 2.40 Nm). The control torque was saved with each iteration of the control loop updating at 250Hz. Each participants' stance strides were parsed heel-strike to toe-off using the FSR and the left and right strides for each participant for each task were averaged together. The task performed during each stride was identified using a video recording of each trial.

The experimental average steady-state strides are compared to steady-state strides from the normative dataset [24]. The strides after the participant reached steady-state were used for each treadmill speed. Due to hardware error, the treadmill strides for s1 at speeds of 1.25 and 0.75 m/s were collected only for the left exoskeleton for a duration of four minutes at each speed to obtain a comparable number of strides. We used the only stair stride occurring heel-strike to heel-strike on the steps as the representative steady-state stair ascent and descent stride. The number of steady-state strides on the ramp depended on each participant's stride length. We defined the steady-state ramp strides as those excluding the first two heel-strikes on the ramp as being transition strides. This definition ensured that each participant achieved at least one steady-state stride on the ramp. The normative data used for comparison were collected at corresponding treadmill speeds and stair step height with the exception of ramp tasks. The normative ramp incline for comparison is 12.4°, which is the closest available comparison in the normative dataset. Stand-to-sit strides were parsed beginning when participants returned to standing in front of the stool and ending when the controller state machine detected a toe-off event (i.e., participant bodyweight offloaded onto the stool).

Although not explicitly trained into the controller, the transition strides between walking and ramp or stairs are also compared to the normative dataset. The s1 stride is defined by the stance leg while the contralateral leg is transitioning between walking and ramp or stairs. The R2W and S2W strides are defined by the stance leg while the contralateral leg is transitioning ramp to walking or stairs to walking, respectively.

TABLE I
PUSH-OFF PEAK COMPARISON

Task (Fig. 5)	Experimental		Normative	
	Phase % Stance	Magnitude Nm/kg	Phase % Stance	Magnitude Nm/kg
0.75 m/s	78.7%	1.4	75.7%	1.2
1 m/s	78.1%	1.7	76.6%	1.4
1.25m/s	79.4%	1.7	77.8%	1.5
14.1° D	75.0%	1.7	76.7%	1.09
14.1° I	76.5%	1.8	78.1%	1.7
7 in SD	74.6%	1.8	76.2%	1.0
7 in SA	78.1%	1.3	79.7%	1.3
s1 D	76.7%	1.9	83.3%	1.4
s1 I	87.5%	1.7	78.1%	1.8
s1 SD	77.8%	1.9	77.8%	1.8
s1 SA	79.7%	1.5	78.1%	1.8
R2W D	83.3%	1.9	78.3%	1.3
R2W I	76.6%	2.0	75.0%	1.6
S2W SD	74.6%	1.9	74.6%	1.6
S2W SA	78.1%	1.3	75.0%	1.7

V. EXPERIMENTAL RESULTS

Experimental and normative push-off peak phase are very similar across all tasks, while magnitude notably overshoots for some tasks (Tab. I). Torque profiles for steady-state walking at each speed align closely with normative, though the peak is consistently higher (Fig. 5.A,B,C). The push-off torque peaks for ramp and stair descent are higher than normative with high variance between subjects during late stance (Fig. 5.E,G). The push-off torque peaks for ramp and stair ascent align closely with normative, though the loading response torque peaks are higher than normative. Steady-state ramp and stair tasks have high variance across subjects. During stand-to-sit the controller applies larger plantarflexion torques (peak $\sim$ 0.70 Nm/kg) compared to normative (peak $\sim$ 0.27 Nm/kg), and there is high variance across subjects.

Considering activity transitions, the s1 strides for ramp incline and stair decline have comparable torque peak magnitude and torque peak timing. The s1 stride for ramp decline

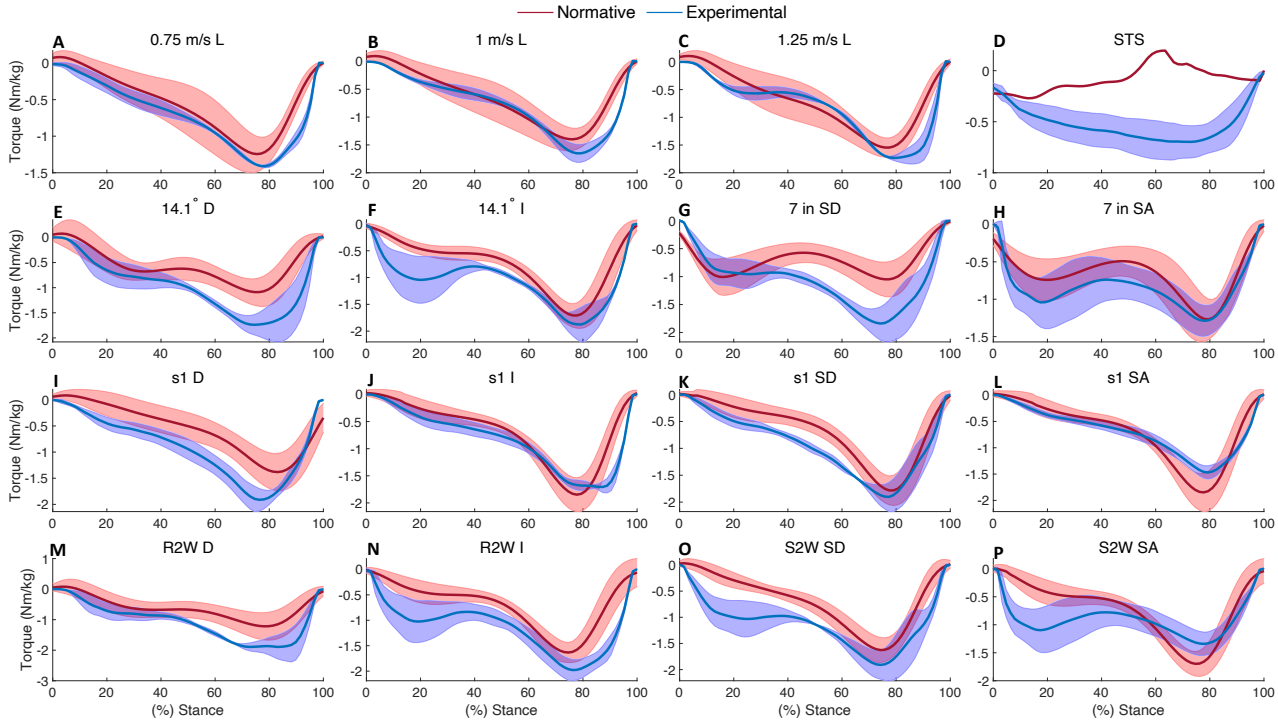

Fig. 5. **Participant average stride** (solid line) **and inter-participant experimental standard deviation** (shaded region) **vs. normative** average subject (solid line) and inter-subject normative standard deviation (shaded region) for the N=12 subjects used in the optimization [24]. Steady-state average strides presented for level walking (L), ramp decline (D), ramp incline (I), stair descent (SD), stair ascent (SA). Stride s1 is defined by the stance leg while the contralateral leg transitions from walking to ramp or walking to stairs. Strides R2W and S2W are defined by the stance leg while the contralateral leg transitions from ramp to walking or stairs to walking, respectively. Stand-to-sit (STS) normative comparison is a single average stride from [27].

has a higher magnitude and is phase-shifted ahead of the normative peak while the s1 stride for stair ascent has a smaller magnitude than normative. The R2W and S2W strides have consistently higher magnitude loading response torque peaks compared to normative across tasks. The R2W and S2W torque peak magnitudes are comparable for ramp incline, stair descent, and stair ascent while the torque peak magnitude for ramp descent is higher than normative.

VI. Discussion

As the most frequent ADL, walking was prioritized with a higher weight in the optimization, and the walking tasks had the best performance across participants. Human-in-the-loop optimization minimizing metabolic cost of gait has resulted in steadily increasing peak torque magnitudes [11], indicating that higher magnitudes compared to normative would benefit the user for walking tasks. The controller torque peak phase lag from normative would also likely benefit the user, as previous studies have shown that metabolic cost is minimized with peaks between 79% and 85% of stance [11], [12]. Though this is a large range of optimized values, all occur after the normative torque peak.

Though the stand-to-sit torque is mismatched from normative, study participants commented either not recognizing the torque mismatch or not noticing additional assistance compared to the average ~ 0.33 Nm/kg supportive plantarflexion torque applied during standing. The high variance between subjects during stand-to-sit could be the result of participants not loading each leg evenly with each repetition.

In ramp and stair tasks, the controller correctly applied torque peaks at the end of loading response and push-off. Several factors could have influenced the high variance for steady-state ramp and stair tasks. Though participants were asked to be consistent across repetitions, stride length and speed were not enforced across subjects. Further, humans have highly variable techniques for climbing stairs (e.g., only making stair contact with the toes or planting the full foot on the step), and the normative data used for comparison may not capture the participants' individual kinematics.

The controller also performed reasonably well for transition strides between walking and ramp or stairs. The controller accurately approximates the torque profiles for s1 strides closely to those for walking and R2W strides closely to those for ramp. However, the controller approximates S2W strides closely to those for stair tasks while normative more closely resembles walking kinetics. It is unclear why normative more closely resembles walking, as S2W is the last stance stride to occur on the stairs. Despite the discrepancy in the magnitude of the loading response torque peak, the higher magnitude push-off torque peak is approximately aligned with normative for S2W strides. These preliminary results suggest that the task-invariant controller optimized on steady-state strides can approximate biomimetic torque for transitions between tasks without task classification.

This proof-of-concept study shows promising results for approximating biomimetic torque with limited sensor inputs, though there is high variation between the small number of study participants. Humans have variable gait

kinematics, with large standard deviations for normative average strides (Fig. 5). It is not reasonable to expect a non-personalized task-invariant controller to perfectly match each user's kinematics. Further, it is not guaranteed that the average normative kinematics presented for comparison in Fig. 5 are representative of the three participants included in this study. However, the experimental results indicate the task-invariant controller can approximate biomimetic torque across tasks. A larger sample size would be required to make firm conclusions about the ability of the controller to generalize to the population.

As the controller depends only on orientation and *vGRF*, the control behavior is consistent for each user's kinematics and there is no risk of unexpected torque due to misclassification of state or task. Adaptation to static torque profiles yields similar benefits to personalized assistance profiles after several hours of training [11]. Thus, despite some variance in magnitudes of torque assistance across tasks compared to normative, it is likely that human adaptation would allow the user to maximize assistance from this controller.

VII. Conclusion

In this paper, we extended the optimal task-invariant energy shaping control approach to a single-joint ankle exoskeleton. This controller used optimized control parameters for intuitively chosen basis functions to approximate biomimetic torque profiles for walking, ramp, and stairs in simulation. Though the control framework is capable of producing both dorsiflexion and plantarflexion torques, the commercially available ankle exoskeleton only applies plantarflexion torques, so we restricted the controller accordingly. A proof of concept experiment with N=3 able-bodied subjects indicated that the controller continues to approximate biomimetic torque profiles across tasks in real hardware, and additionally handles task transitions which were outside the training set.

Acknowledgement

The authors thank Nikhil V. Divekar and Elliott J. Rouse for their assistance.

References

[1] M. Meinders, A. Gitter, and J. M. Czerniecki, "The role of ankle plantar flexor muscle work during walking." *Scand J Rehab Med*, vol. 30, no. 1, pp. 39–46, 1998.

[2] B. R. Umberger and J. Rubenson, "Understanding muscle energetics in locomotion: new modeling and experimental approaches," *Exerc Sport Sci Rev*, vol. 39, no. 2, pp. 59–67, 2011.

[3] G. S. Sawicki, O. N. Beck, I. Kang, and A. J. Young, "The exoskeleton expansion: improving walking and running economy," *J NeuroEngineering Rehabil*, vol. 17, no. 1, pp. 1–9, 2020.

[4] K. E. Gordon and D. P. Ferris, "Learning to walk with a robotic ankle exoskeleton," *J Biomech*, vol. 40, no. 12, pp. 2636–2644, 2007.

[5] J. R. Koller, D. A. Jacobs, D. P. Ferris, and C. D. Remy, "Learning to walk with an adaptive gain proportional myoelectric controller for a robotic ankle exoskeleton," *J NeuroEngineering Rehabil*, vol. 12, no. 1, pp. 1–14, 2015.

[6] R. W. Jackson and S. H. Collins, "Heuristic-based ankle exoskeleton control for co-adaptive assistance of human locomotion," *IEEE Trans Neural Syst Rehabil Eng*, vol. 27, no. 10, pp. 2059–2069, 2019.

[7] D. Comaduran Marquez, V. von Tscharner, K. Murari, and B. M. Nigg, "Development of a multichannel current-emg system for coherence modulation with visual biofeedback," *PloS one*, vol. 13, no. 11, p. e0206871, 2018.

[8] P. Malcolm, W. Derave, S. Galle, and D. De Clercq, "A simple exoskeleton that assists plantarflexion can reduce the metabolic cost of human walking," *PloS one*, vol. 8, no. 2, p. e56137, 2013.

[9] S. Galle, P. Malcolm, S. H. Collins, and D. De Clercq, "Reducing the metabolic cost of walking with an ankle exoskeleton: interaction between actuation timing and power," *J NeuroEngineering Rehabil*, vol. 14, no. 1, pp. 1–16, 2017.

[10] S. Lee, S. Crea, P. Malcolm, I. Galiana, A. Asbeck, and C. Walsh, "Controlling negative and positive power at the ankle with a soft exosuit," in *IEEE Int Conf Robot Automation*, 2016, pp. 3509–3515.

[11] K. L. Poggensee and S. H. Collins, "How adaptation, training, and customization contribute to benefits from exoskeleton assistance," *Science Robotics*, vol. 6, no. 58, p. eabf1078, 2021.

[12] J. Zhang, P. Fiers, K. A. Witte, R. W. Jackson, K. L. Poggensee, C. G. Atkeson, and S. H. Collins, "Human-in-the-loop optimization of exoskeleton assistance during walking," *Science*, vol. 356, no. 6344, pp. 1280–1284, 2017.

[13] R. W. Jackson and S. H. Collins, "An experimental comparison of the relative benefits of work and torque assistance in ankle exoskeletons," *J Appl Physiol*, vol. 119, no. 5, pp. 541–557, 2015.

[14] P. Slade, M. J. Kochenderfer, S. L. Delp, and S. H. Collins, "Personalizing exoskeleton assistance while walking in the real world," *Nature*, vol. 610, no. 7931, pp. 277–282, 2022.

[15] M. K. Shepherd, D. D. Molinaro, G. S. Sawicki, and A. J. Young, "Deep learning enables exoboot control to augment variable-speed walking," *IEEE Robot Autom Lett*, vol. 7, no. 2, pp. 3571–3577, 2022.

[16] K. Seo, Y. J. Park, J. Lee, S. Hyung, M. Lee, J. Kim, H. Choi, and Y. Shim, "Rnn-based on-line continuous gait phase estimation from shank-mounted imus to control ankle exoskeletons," in *IEEE Int Conf Rehabil Robot*, 2019, pp. 809–815.

[17] C. Khazoom, C. Véronneau, J.-P. L. Bigué, J. Grenier, A. Girard, and J.-S. Plante, "Design and control of a multifunctional ankle exoskeleton powered by magnetorheological actuators to assist walking, jumping, and landing," *IEEE Robot Autom Lett*, vol. 4, no. 3, pp. 3083–3090, 2019.

[18] R. L. Medrano, G. C. Thomas, C. G. Keais, E. J. Rouse, and R. D. Gregg, "Real-time gait phase and task estimation for controlling a powered ankle exoskeleton on extremely uneven terrain," *IEEE Trans Robotics*, 2023.

[19] S. S. P. A. Bishe, T. Nguyen, Y. Fang, and Z. F. Lerner, "Adaptive ankle exoskeleton control: Validation across diverse walking conditions," *IEEE Trans Med Robot Bionics*, vol. 3, no. 3, pp. 801–812, 2021.

[20] B. He, G. C. Thomas, N. Paine, and L. Sentis, "Modeling and loop shaping of single-joint amplification exoskeleton with contact sensing and series elastic actuation," in *2019 American Control Conference (ACC)*. IEEE, 2019, pp. 4580–4587.

[21] G. Lv, H. Zhu, T. Elery, L. Li, and R. D. Gregg, "Experimental implementation of underactuated potential energy shaping on a powered ankle-foot orthosis," in *IEEE Int Conf Robot Automation*, 2016, pp. 3493–3500.

[22] J. Lin, N. V. Divekar, G. Lv, and R. D. Gregg, "Optimal task-invariant energetic control for a knee-ankle exoskeleton," *IEEE Control Systems Letters*, vol. 5, no. 5, pp. 1711–1716, 2021.

[23] J. Lin, N. V. Divekar, G. C. Thomas, and R. D. Gregg, "Optimally biomimetic passivity-based control of a lower-limb exoskeleton over the primary activities of daily life," *IEEE Open J Control Syst*, vol. 1, pp. 15–28, 2022.

[24] J. Camargo, A. Ramanathan, W. Flanagan, and A. Young, "A comprehensive, open-source dataset of lower limb biomechanics in multiple conditions of stairs, ramps, and level-ground ambulation and transitions," *J Biomech*, vol. 119, p. 110320, 2021.

[25] R. Macaluso, K. Embry, D. J. Villarreal, and R. D. Gregg, "Parameterizing human locomotion across quasi-random treadmill perturbations and inclines," *IEEE Trans Neural Syst Rehabil Eng*, vol. 29, pp. 508–516, 2021.

[26] M. Grant and S. Boyd, "CVX: Matlab software for disciplined convex programming, version 2.1," http://cvxr.com/cvx, Mar. 2014.

[27] B. Laschowski, R. S. Razavian, and J. McPhee, "Simulation of stand-to-sit biomechanics for robotic exoskeletons and prostheses with energy regeneration," *IEEE Trans Med Robot Bionics*, vol. 3, no. 2, pp. 455–462, 2021.